A novel semi-batch autoclave reactor to overcome thermal dwell time in solvent liquefaction experiments

Jake K. Lindstrom,[a] Jessica L. Brown,[a,b] Chad A. Peterson,[a,b] Arpa Ghosh,[a] Sean A. Rollag,[a,c] Panos D. Kouris,[d,e] Michael D. Boot,[d,f] Emiel J.M. Hensen,[d,e] Preston Gable,[a] Ryan G. Smith,[a] Robert C. Brown[a,b,c*]

a- Bioeconomy Institute, Iowa State University, Ames, IA, 50011, United States of America

b- Department of Mechanical Engineering, Iowa State University, Ames, IA, 50011, United States of America

c- Department of Chemical and Biological Engineering, Iowa State University, Ames, IA, 50011, United States of America

d- Vertoro B.V., Geleen, The Netherlands

e- Department of Chemical Engineering and Chemistry, Eindhoven University of Technology, Eindhoven, The Netherlands

f- Department of Mechanical Engineering, Eindhoven University of Technology, Eindhoven, The Netherlands

*Corresponding author: Email address: rcbrown3@iastate.edu (R.C. Brown)

Postal address: 1140E Biorenewables Research Laboratory, 617 Bissell Rd, Ames, IA 50011

Abstract

The thermal profile of solvent liquefaction experiments must be well-controlled to generate data suitable for process scaling and technoeconomic analysis. Acknowledging the differences in small-scale batch systems compared to continuous commercial processes is important. In particular, many experiments have long heating and cooling periods, which influence rates of reaction in ways that would not occur in commercial continuous reactors. To overcome this problem, a novel semi-batch autoclave (SBA) system was built to rapidly heat reactants and cool products while maintaining constant pressure during solvent liquefaction experiments. In this study, the performance of the SBA reactor was compared to an isobaric conventional batch autoclave (ICBA) reactor in the solvent liquefaction of lignin in n-butanol. Heat transfer affected both the apparent reaction rate and measured product yields. Solvent liquefaction limited by slow heating gave the misperception that reaction rates were faster than was actually the case and promoted the formation of char-like solids. Experiments constrained by slow heat transfer are of limited use in process modeling and reactor design, which would otherwise result in undersized reactors for desired processing rates. The SBA system facilitates the design and scale-up of commercial SL plants as it approximates the thermal profile of a continuous system.

Keywords

Solvent liquefaction; heat transfer; lignin; biorefinery; process development

1. Introduction

Solvent liquefaction (SL) is the conversion of organic matter in hot, pressurized solvent to produce solubilized compounds, gases, and solid residue [1]. Lignocellulosic biomass, extracted lignin, animal manure, sewage sludge, and algal biomass are potential feedstocks for SL [1–4]. Advantages compared to other kinds of thermochemical conversion of biomass include the ability to process wet wastes (especially when water is the solvent) and generally higher yields, selectivity, and quality of liquid products compared to pyrolysis [1]. Notably, the yield of char-like solid from solvent liquefaction of lignocellulosic biomass is generally much lower than the yield of char from pyrolysis [5–7].

Continuous reactors are usually preferred for commercial processes, providing advantages in throughput and operating costs compared to batch reactors [8]. However, laboratory research in solvent liquefaction, which requires operation at high pressure, has mostly been performed in batch reactors [6–12] because of their lower capital cost and simplicity of operation compared to continuous reactors [9]. Batch reactors include tubular reactors and autoclave reactors.

The low cost and small size of tubular reactors allows multiple trials to be performed simultaneously, with the reactors rapidly heated by immersion in a sand bath or hot oil. However, they suffer from poor mixing of reactants, which introduces potential mass transfer limitations to the process. Using appropriate diluents, keeping biomass-to-solvent ratio small, and/or shaking the reactor can mitigate this problem [10–12].

Autoclave reactors, as they are conventionally employed in solvent liquefaction experiments, are true batch reactors with no transfer of reactants or products to or from the reactor during an experiment. Although some autoclave manufacturers include provisions for

injecting or extracting liquid samples into or out of these otherwise sealed reactors, this does not include conveyance of solid reactants or products. These conventional batch autoclave (CBA) reactors often include internal impellers for the purpose of mitigating mass transfer limitations. However, the high thermal mass of these sealed pressure vessels severely limits heating rates to about 5ºC min^{-1},[3] potentially leading to heat transfer limited reaction rates [3,6,13–17]. Similarly, the high thermal mass prevents rapid cooling, resulting in reactions proceeding longer than desired [3,6,13–16].

For an experiment, a CBA is preloaded with solvent and reactant, sealed and pressurized, then heated to the desired reaction temperature using ceramic heaters or heat tape surrounding the reactor. The mass of these pressure vessels usually precludes rapid heating, requiring up to 30 minutes to reach desired operating temperature, as routinely reported in the literature [3,6,13–17]. Similarly, cooling at the end of an experiment is very slow, accomplished by removing the heaters and exposing the reactor shell to air flow from a fan for initial cooling followed by immersion in cold water. Elapsed time from the end of the experiment until the reactor is cool enough to vent and open can approach an hour. Despite the prolonged heating and cooling times, researchers using CBAs usually define reaction time as the time interval between the reactor reaching the set point temperature and the time at which cooling of the reactor begins [3,6,13,16,17]. In fact, the slurry may spend more time exposed to the temperature ramps associated with heating and cooling the reactor than at the set point temperature [18]. This extended exposure to elevated temperatures likely affects product yields and makes it difficult to collect meaningful rate data. Although the limitations of using autoclave reactors in solvent liquefaction experiments have long been acknowledged [19,20], they are still commonly employed.

Prolonged temperature ramps undoubtedly influence conversion of reactants and yields of products [18]. For example, Kumar et al. [18] found that fast heating increased liquid yields for solvent liquefaction of pine wood. Brodzki et al. [21] performed coal liquefaction in tetralin and found that slow heating in an autoclave resulted in secondary decomposition reactions not observed in experiments with a continuous flow reactor. Thus, autoclave reactors as conventionally heated can produce results that do not accurately portray isothermal operation of a solvent liquefaction process.

Furthermore, much of the research using autoclave reactors for solvent processing do not control for pressure, which increases during heating and decreases during cooling. Pressure is known to influence product yields and reaction rates [22]. Haverly et al. [3,6] made improvements in this respect by adding a gas exhaust line connected to a condenser via a pressure regulator, resulting in an isobaric conventional autoclave (ICBA) reactor, which vented gases and vapors as they were generated.

The systematic errors associated with the use of CBAs in solvent liquefaction studies are likely to have major ramifications in the design of continuous reactors for commercial applications. The slower heating and cooling rates in CBAs compared to continuous reactors are expected to underestimate product yields that could be achieved in continuous reactors [18,21], resulting in overly pessimistic estimates of the economic performance of a commercial plant, thus discouraging investment. On the other hand, the exclusion of heating and cooling times from reaction rate calculations can inflate apparent reaction rates, which could lead to an undersized reactor design, as higher reaction rates decrease reactor volume for a given biomass throughput. Although common practice ignores thermal lag, its exclusion would provide an overly optimistic reactor cost estimate, thus inflating investment prospects. Together, these

issues only serve to confound economic estimations. Quantifying these errors is important in advancing the commercial prospects for solvent liquefaction.

We have developed a novel semi-batch autoclave (SBA) system that overcomes the prolonged heating and cooling periods associated with solvent liquefaction in CBAs as well as maintains constant pressure during the process. The SBA injects a slurry of biomass and solvent into a preheated reactor and, at the end of the desired residence time, ejects the slurry into a pre-chilled quench vessel. Because the SBA rapidly heats reactants and cools products, it is able to simulate the thermal profile of a continuous plug flow reactor. In contrast, thermal management of an CBA is constrained by its large thermal mass.

To bring clarity to the definition of reaction time, we distinguish between nominal reaction time and thermal dwell time in the experiments. For the ICBA, nominal reaction time is the time the slurry spends at the desired set point temperature. Nominal reaction time corresponds to the reaction time employed by most previous CBA researchers despite its obvious limitations in describing the time reactants are exposed to elevated temperatures. We define thermal dwell time as the non-isothermal interval between the start of reactor heating and the completion of reactor cooling [3,13,16,17]. For the SBA, nominal reaction time is the interval between reactants being injected into and ejected from the reactor. As we will see, this time also corresponds closely to the time the slurry resides at the set point temperature. For both the ICBA and SBA, thermal dwell time includes heating and cooling times and the nominal reaction time.

In this study, isobaric solvent liquefaction of lignin in butanol is compared for SBA and ICBA reactor configurations. Comparison of results for these two reactor systems allows the effects of heating and cooling rates on solvent liquefaction to be evaluated. Product yields were compared between nominal reaction times and thermal profiles of the ICBA and novel SBA.

Thermal dwell time proved tremendously influential in this study, with prolonged times leading to multiple significant challenges.

2. Methodology

2.1 Feedstock

The technical lignin used in this study was Omno™, produced by Renmatix as a byproduct of supercritical hydrolysis of lignocellulose [23]. Renmatix Omno lignin feedstock was determined to have a total ash content of 0.050 ± 0.046 wt%, according to proximate analysis performed in a Mettler-Toledo TGA. Prior to SL experiments, lignin was ground in a Retsch planetary ball mill (PM 100) at 300 rpm for 30 minutes (comprised of 10 minutes of grinding, 10 minutes of cool down, followed by 10 more minutes of grinding) to obtain a powder of less than 100 μm particle size.

The solvent used in SL trials was n-butanol. Four-liter bottles of reagent grade (<99.4% purity) were purchased from Thermo Fischer Scientific. Both the SBA and ICBA trials used 250 mL of n-butanol and 25 g of lignin. Control trials were performed by mixing 100 mL of butanol with 10 g lignin, maintaining the same solvent to lignin ratio, and holding the mixture at room temperature for 30 minutes before analyzing the products in a manner similar to that employed for SBA and ICBA trials.

2.2 Isobaric conventional batch autoclave reactor (ICBA)

The ICBA, illustrated in Figure 1, consisted of a 500 mL Autoclave Engineers EZE-Seal® stirred pressure vessel with provisions for isobaric operation. The system was modified to incorporate high-pressure handling of volatile products through an overheads condenser, chilled to -5°C, which collected all condensable products. A backpressure regulator automatically

controlled system pressure. A 470 W heat tape covering the reactor flange and a 1000 W clamshell heater surrounding the vessel were used to bring the ICBA to reaction temperature. Further details on the construction of a previous version of the ICBA are found in Haverly et. al. [3].

For each experiment, the ICBA was loaded with 25 g of lignin and 250 mL of n-butanol, sealed and purged with nitrogen, and heated to reaction temperature. The heater output during initial heating was controlled manually, but once the desired temperature was achieved, a proportional–integral–derivative (PID) control system was used to regulate temperature supplemented with intermittent operator control. The pressure and temperature data for every experiment was logged using PI Coresight from OSIsoft.

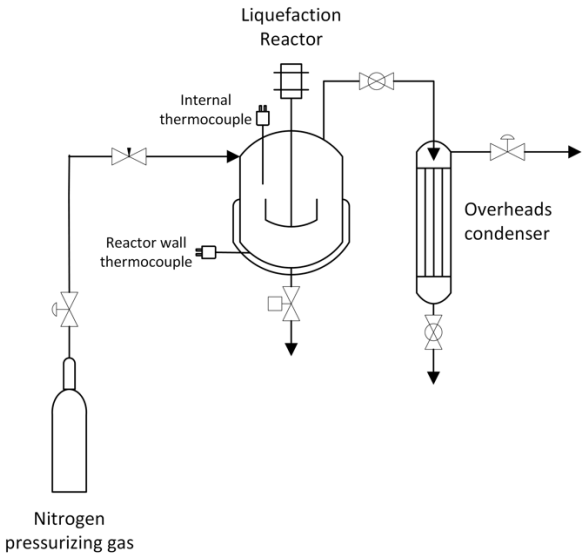

Figure 1. Block flow diagram of the isobaric conventional autothermal reactor system with high-pressure overheads handling to achieve constant pressure operation. A thermocouple imbedded in the reactor wall was used to regulate temperatures, and an internal thermocouple allowed for monitoring of the temperature of the reactor and its contents.

In ICBA trials, the nominal reaction time began when the internal temperature reached 200°C, measured with an internal thermocouple noted in Figure 1. After the desired nominal reaction time, the insulation and heaters were removed, and a large fan was directed toward the

reactor to enhance convective cooling. Once the internal temperature cooled to 100°C, the entire reactor system was depressurized through the overheads condenser to collect any additional vapor products. The ICBA was then opened and condensed-phase products were removed via a drain port at the bottom of the reactor.

2.3 Semi-batch autoclave (SBA)

As shown in Figure 2, the SBA consists of a slurry feeder in the form of a 300 mL 316 stainless steel Bolted Closure pressure vessel, a liquefaction reactor constructed from a 500 mL 316 stainless steel EZE-Seal® pressure vessel, a bottom (liquid) quench vessel, and an overheads (vapor) condenser vessel. Both the slurry feeder and the liquefaction reactor were obtained from Autoclave Engineers. The bottoms quench consisted of a 1000 mL stainless steel Swagelok vessel. In preparation for an experiment, the slurry feeder was loaded with 250 mL of n-butanol and 25 g of lignin, which was then sealed, purged with nitrogen, and pressurized to 500 psi (34.5 bar). The liquefaction reactor was pressurized to 200 psi (13.8 bar). The slurry feeder was connected to the liquefaction reactor via a pneumatically actuated ball valve and a 0.25-inch stainless steel transfer line of 36-inch length. The preheat temperature of the liquefaction reactor was selected such that its thermal mass rapidly heated the entering slurry to the set point temperature while a backpressure regulator automatically controlled pressure in the liquefaction reactor. The liquefaction reactor was preheated to 250°C, which is 50°C higher than the desired set point temperature of 200°C. The preheat temperature was determined from both thermodynamic calculations[24] and experimental data (see Electronic Supplemental Information section 1).

Once preheat was achieved, the valve between the slurry and liquefaction reactors was opened, which rapidly discharged the slurry from the slurry feeder to the liquefaction reactor.

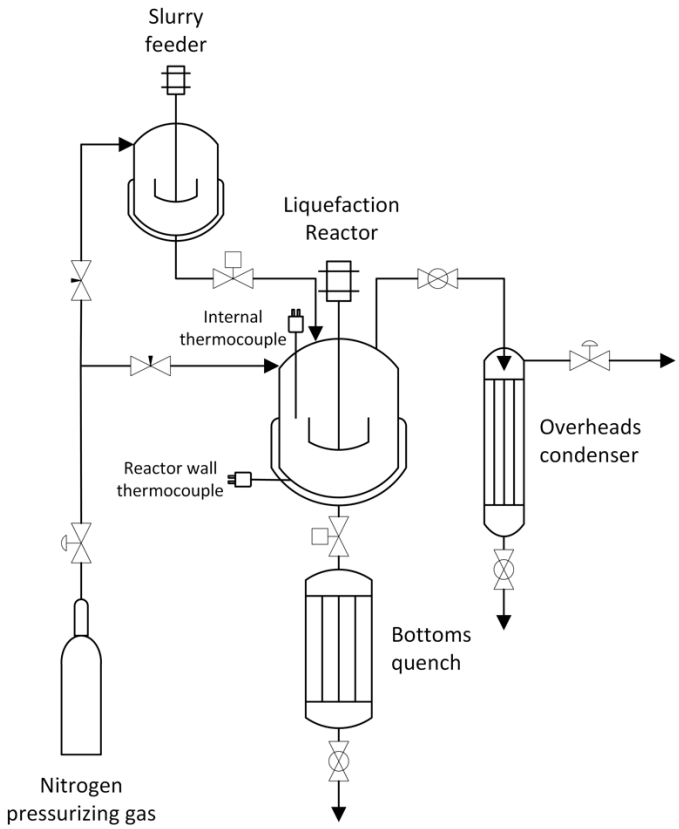

Figure 2. Block flow diagram of the semi-batch autoclave reactor system used to achieve rapid heating and cooling of reactant/product mixtures during solvent liquefaction experiments. A thermocouple within a thermowell inserted into the top of the reactor measured the internal temperature of the reactor and its contents.

Considering the very rapid heating and cooling achieved in the SBA, nominal reaction time for this reactor is defined as the time interval between slurry injection into the liquefaction reactor and its expulsion. The thermal mass of the preheated liquefaction reactor wall rapidly transferred heat to the slurry upon injection. Once the internal temperature was within 10 °C of the set point temperature, a PID controller maintained the liquefaction reactor at this temperature. PI Coresight from OSIsoft was used for data logging. Volatile products continuously passed through the chilled overheads condenser where they were recovered as liquids. After a prescribed nominal reaction time, the slurry was ejected from the liquefaction reactor through a pneumatically actuated ball valve and stainless steel transfer line of 3/8-inch I.D. and 9.5-inch length into the pre-chilled bottoms quench.

The thermal profile of the SBA for the slurry after injection into the liquefaction reactor was determined through a composite of readings from thermocouples located in three distinct zones of the reactor system. The slurry feeder was not heated and therefore considered to be at room temperature. The overall temperature profile was produced by combining the slurry feeder temperature, internal reactor thermocouple, and internal bottoms quench thermal profiles, as shown in Figure 3a. These three thermal profiles were combined to form the slurry thermal profile, shown in Figure 3b, by following the path of slurry through the SBA system. For the SBA, the wall and slurry of the liquefaction reactor rapidly converge toward a common temperature and the slurry reach the set point temperature in only 5 minutes.

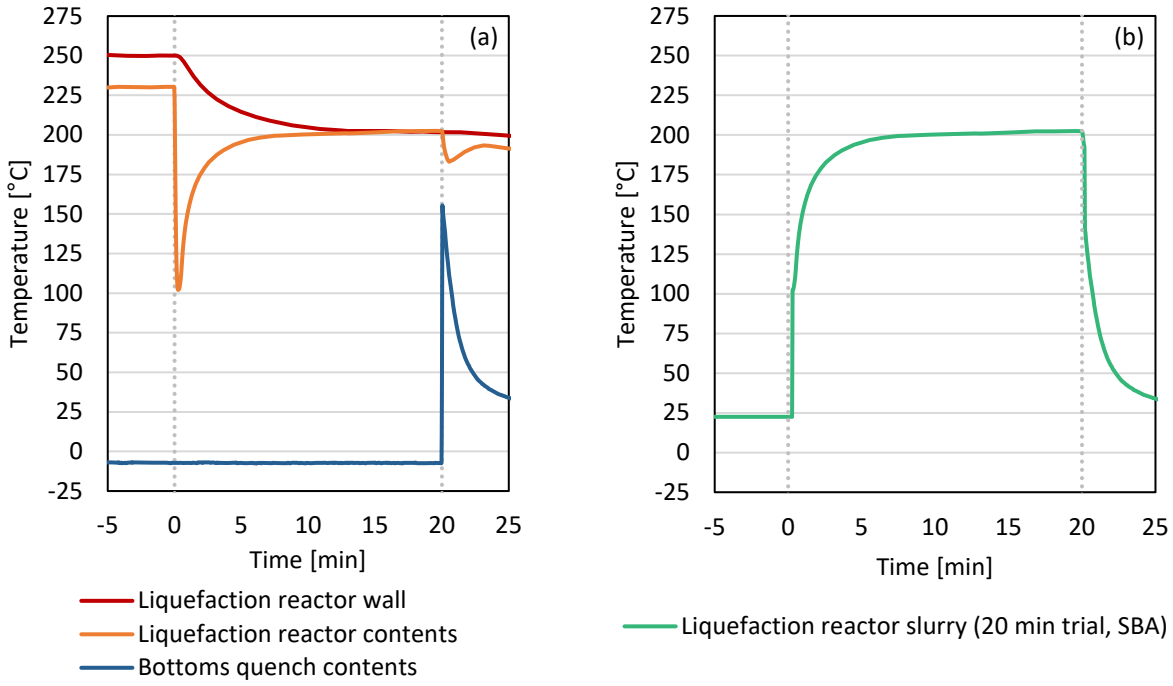

Figure 3. Temperature profiles in the SBA for a test with a 20-minute nominal reaction time using 25 g of lignin in 250 mL of n-butanol. (a) Temperature of liquefaction reactor wall and its contents and bottoms quench contents; (b) slurry temperature profile in liquefaction reactor developed from a composite of other temperature profiles.

After depressurization, the slurry feeder was removed and weighed along with any residual solvent and lignin remaining in this vessel. The open slurry feeder was dried to

evaporate residual solvent and allow an accurate measurement of the mass of residual lignin. The mass of residual solvent was determined by difference. The mass of lignin received from the slurry feeder by the liquefaction reactor was determined by subtracting the feeder's residual lignin mass from the mass of lignin originally loaded in the feeder. The liquefaction products and solvent collected in the condenser and bottoms quench were analyzed separately.

2.4 ICBA and SBA Product Analyses

Volatile products (termed "overheads") collected in the overheads condenser were collected in pre-weighed bottles. Analysis of overheads showed that only solvent was present; no evidence of other volatiles was found. The mixture of products from the bottoms quench was termed "bottoms" and contained solvent, solubilized compounds, and suspended solids. After collection of bottoms in a pre-weighed bottle, the bottoms quench was then filled with one liter of methanol to wash out any residue on the walls. Liquid from this washing step was collected and termed "bottoms wash." Products were stored at 4 °C when not in use. The separations and analyses processes are illustrated in Figure 4. The product from the control trials was treated as "bottoms" for separation and analyses. (All mass balances are included in the Electronic Supplemental Information section 2.)

The bottoms were vacuum filtered to remove solids from the mixture. Fifteen milliliters of the raffinate, a mixture of solvent and solubilized compounds, was distilled using a vacuum oven at 55°C with a pressure of 2.6 psi (0.18 bar) for approximately 72 hours to remove n-butanol. The precipitated material remaining after removal of solvent, termed "process-solubilized lignin," was subjected to GC-MS and GPC analyses.

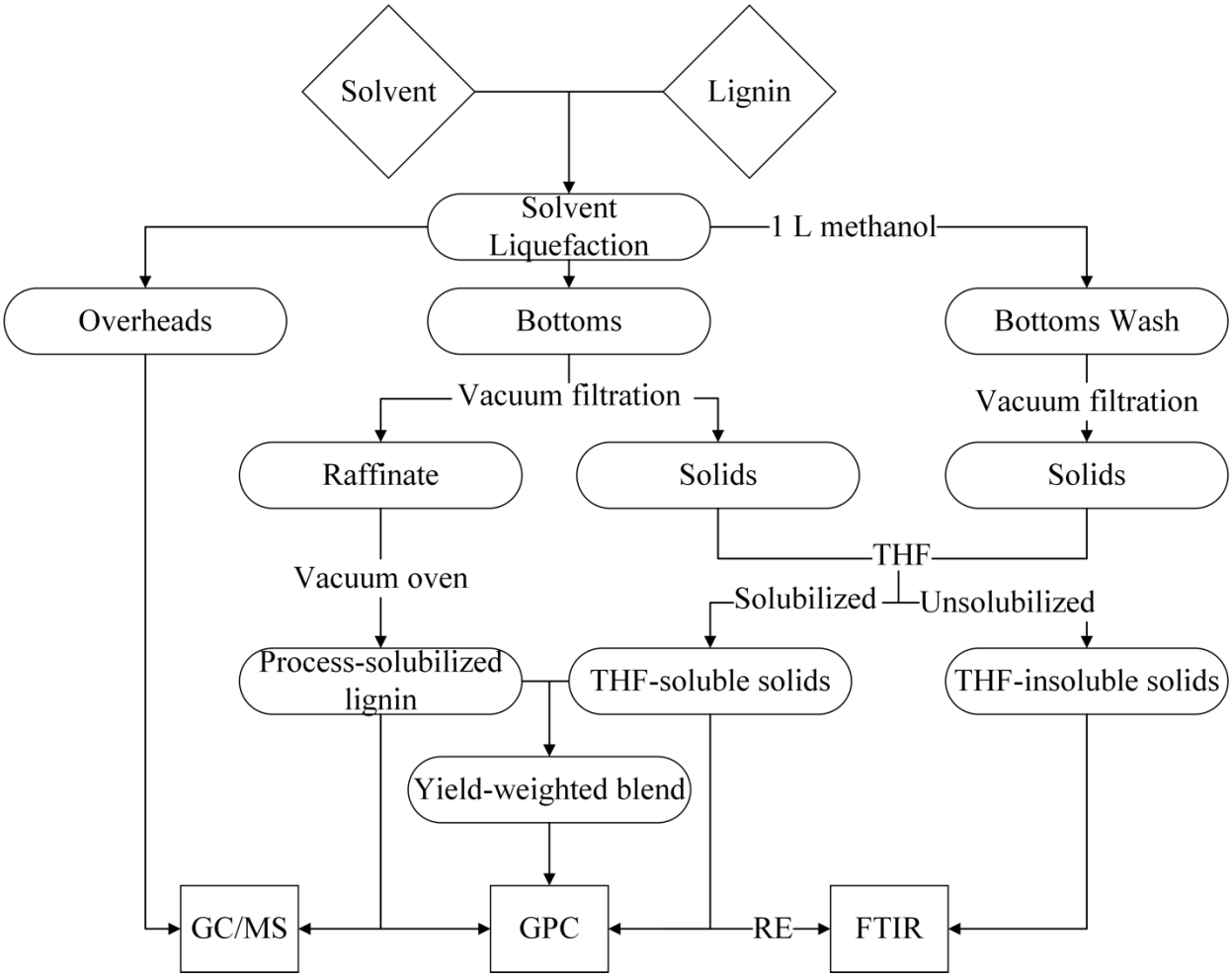

Figure 4. The procedural diagram shows SL reaction, separation, and analyses scheme. Note: RE on the diagram indicates rotary evaporation.

Solids remaining on the filter after vacuum filtration were dried in an oven at 105°C for two hours. The bottoms wash was similarly vacuum filtered and distilled to recover additional process-solubilized lignin. Likewise, the products from the control tests were vacuum filtered to remove solids from the mixture. Filtrate mass was determined by the difference between initial and final filter mass. The yield of "process-solubilized lignin", Y_{PSL}, was determined from the equation:

$$Y_{PSL} = (M_L - M_S)/M_L \qquad (1)$$

where M_L denotes the mass of fed lignin and M_S represents the mass of dried solids.

THF is well known to be an excellent solvent for raw lignin.[1] In fact, we found that the technical lignin used in our experiments was completely soluble in THF. We exploited this phenomenon to determine whether the solids recovered from vacuum filtration contained unreacted or only slightly modified lignin (vs char-like solids from lignin decomposition). Solids that readily dissolved in THF were termed "THF-soluble solids" and were analyzed using GPC and Fourier-Transform Infrared Spectroscopy (FTIR). Before FTIR analysis, THF-soluble solids were subjected to rotary evaporation to remove THF. That part of the solids was not soluble in THF was termed "THF-insoluble solids." The mass of the THF-insoluble solids was measured, and the yield of THF-insoluble solid, Y_{TIS}, was determined according to:

$$Y_{TIS} = M_{TIS}/M_L \quad (2)$$

where M_L denotes the mass of fed lignin and M_{TIS} represents the mass of THF-insoluble solids.

2.5 Gel Permeation Chromatography

The process-solubilized lignin and THF-soluble solids from a SL experiment were separately dissolved in THF [25]. The THF-insoluble solids were not analyzed via gel permeation chromatography (GPC) because products are required to be dissolved in THF for this analysis. Dissolved process-solubilized lignin and THF-soluble solids were analyzed separately via GPC. Additionally, these two solutions were combined in the same ratio as their individual product yields to average the contributions of each of these to the total solubilized products of SL. This blended mixture was named "yield-weighted blend." GPC analysis was performed on the samples by using a Dionex Ultimate 3000 high performance liquid chromatograph. Using THF as the mobile phase, one MesoPore column (3 µm inner diameter, 300 x 7.5 mm; 200 – 25,000 Da) and two Agilent PLgel columns (3 µm inner diameter, 300 x 7.5 mm; 100 – 4000

Da) were used in series. Measurements were performed on the samples using a Shodex Refractive Index (RI) and Diode Array Detector (DAD).

2.6 Gas Chromatography-Mass Spectrometry/Flame Ionization Detector

The overheads and process-solubilized lignin samples were analyzed for monomers using gas chromatography (GC) with a mass spectrometer (MS) and flame ionization detector (FID). An Agilent 7890B GC-MS/FID was used with the methodology from Ghosh et al. [12] Mass spectral peaks were identified using the NIST 2011 library.

2.7 Fourier-Transform Infrared Spectroscopy

THF-soluble solids and THF-insoluble solids were analyzed using Fourier-Transform Infrared Spectroscopy (FTIR). Each sample was scanned 64 times from 4000 cm^{-1} to 525 cm^{-1} with resolution of 4 cm^{-1}. A Thermo Scientific Smart iTR Nicolet iS10 instrument fitted with a diamond window was used for FTIR.

3. Results and Discussion

3.1 Thermal performance of ICBA vs. SBA

The ICBA and SBA systems were operated under identical conditions except for differences in heating and cooling rates imposed by their respective designs. All liquefaction experiments were performed at 200°C except for experiments at room temperature to serve as control trials. The reaction temperature of 200°C was based in part by work performed by Kouris et. al. [26,27].

To evaluate the effect of different heating rates, three nominal reaction times were chosen: 0, 10, and 20 minutes. ICBA experiments with nominal reaction times of zero minutes are experiments in which cooling of the autoclave commenced immediately upon reaching the

set-point temperature. SBA experiments with nominal reaction times of zero minutes represent experiments in which the valve between the liquefaction reactor and the bottoms quench remained open, allowing slurry injected into the liquefaction reactor to flow directly to the bottoms quench. More precisely, the nominal reaction time is a few seconds, which we approximate as zero minutes. Experiments were performed in duplicate for both reactor systems for each nominal reaction time.

The temperature profiles of slurries for nominal reaction times of 0, 10, and 20 minutes are compared for the ICBA and SBA systems in Figure 5. In the SBA, the slurry heated rapidly, mimicking the heat profile of a continuous reactor, as shown in Figure 5a. Once the set point temperature was reached, the temperature of the liquefaction reactor was held constant, similar to steady state conditions reached by a fluid flowing through a plug flow reactor. After ejection into the bottoms quench, the slurry showed a rapid exponential decay in temperature, quickly cooling below ambient temperature. In contrast, the ICBA required 20 minutes to heat the slurry from room temperature to 200°C, as shown in Figure 5b. After reaching the desired nominal reaction time, convective cooling required 20 minutes to cool the slurry below 100°C.

Heating rate for the reactors was defined in terms of the time required to reach 90% of the desired 200°C set point temperature starting from room temperature. Cooling rate was defined in terms of the time required to lower the temperature of the slurry from 200°C to 100°C. Heating and cooling rates in the SBA were 75.6 ± 4.6 °C min^{-1} and -164 ± 6 °C min^{-1}, respectively, while heating and cooling rates for the ICBA were only 9.00 ± 0.31 °C min^{-1} and -4.14 ± 0.13 °C min^{-1}, respectively (uncertainty expressed as standard error).

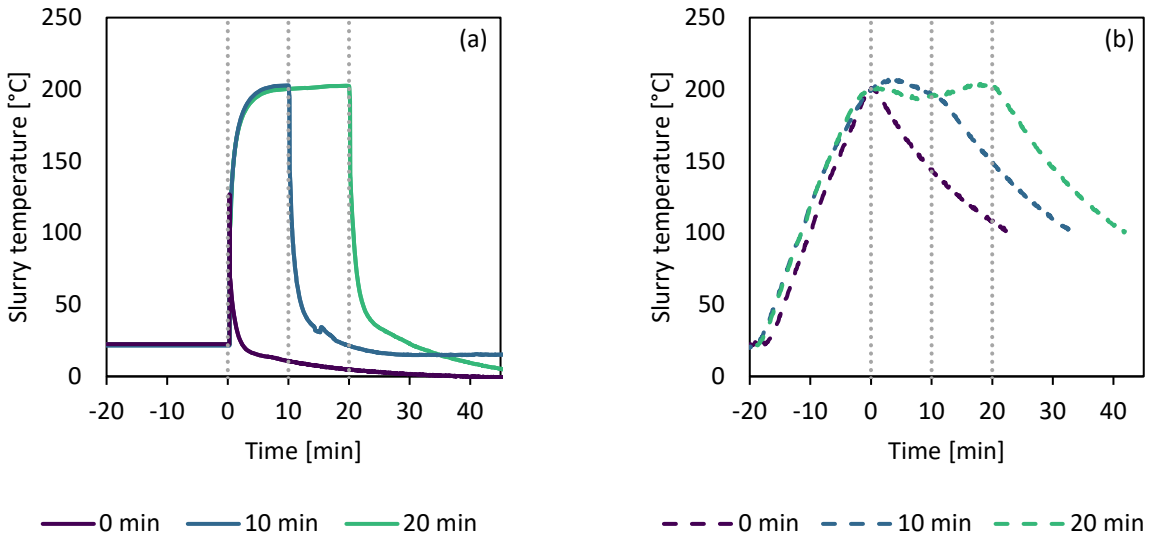

Figure 5. Comparing temperature profiles of slurries (25 g of lignin in 250 mL of n-butanol) in the two reactor systems for three nominal reaction times (0, 10, and 20 minutes) for: (a) the SBA heated slurries to the set point temperature in about 3 minutes and cooled slurries below 100°C almost instantaneously; (b) the ICBA required almost 20 minutes to heat slurries to the set point temperature of 200°C and required similar time to cool slurries below 100°C.

The SBA system relies on the thermal mass of the reactor to heat the slurry once injected. Figure 6a shows how the thermal mass of the reactor provides most of the energy required to heat the slurry. The heater is only applied again later to maintain the desired temperature. This method has the added benefit of providing a large temperature gradient between the vessel wall and slurry, which improves heat transfer rates. In contrast, the thermal energy for the ICBA was provided directly from the electrical heaters. ICBA heating proved more difficult to control, as illustrated in Figure 6b owing to thermal lag between the clamshell heater and the reactor wall and between the reactor wall and the slurry. Prolonged heating and cooling periods during ICBA trials also contributed to the difficulty of temperature control. In addition to higher heating rates, the SBA provided more repeatable thermal profiles than the ICBA. This result likely stems from using simple first-order heat transfer instead of a dynamic temperature control as was done with the ICBA. Additionally, maintaining isothermal conditions with the ICBA was challenging as the PID parameters were tuned for quick and repeatable temperature ramps, not constant reaction

temperatures. To combat instability in ICBA liquefaction reactor contents temperature, manual operator commands interceded the PID controller. Figure 7 compares the thermal profiles for two SBA and two ICBA trials.

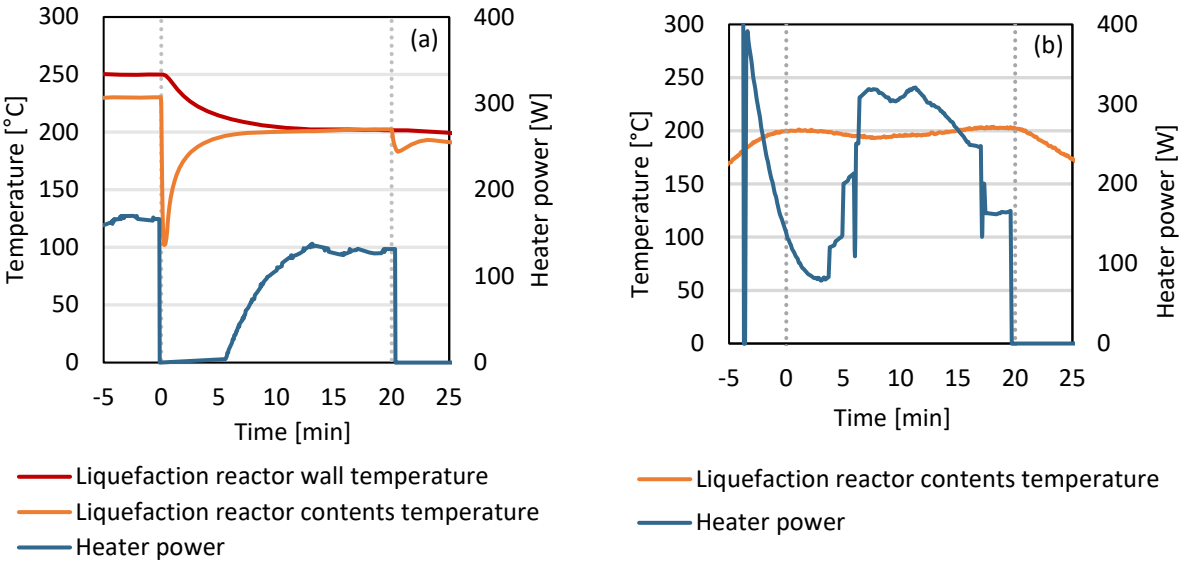

Figure 6. Temperature profiles and heater power for the two solvent liquefaction reactors during 20-minute nominal reaction time test of 25 g of lignin in 250 mL of n-butanol. (a) SBA reactor rapidly heats slurry to the set point temperature of 200°C even before heaters are turned on, demonstrating the important role of reactor thermal mass in controlling temperature; (b) ICBA reactor struggles to hold the set point temperature of 200°C, accompanied by large swings in electric power to the reactor.

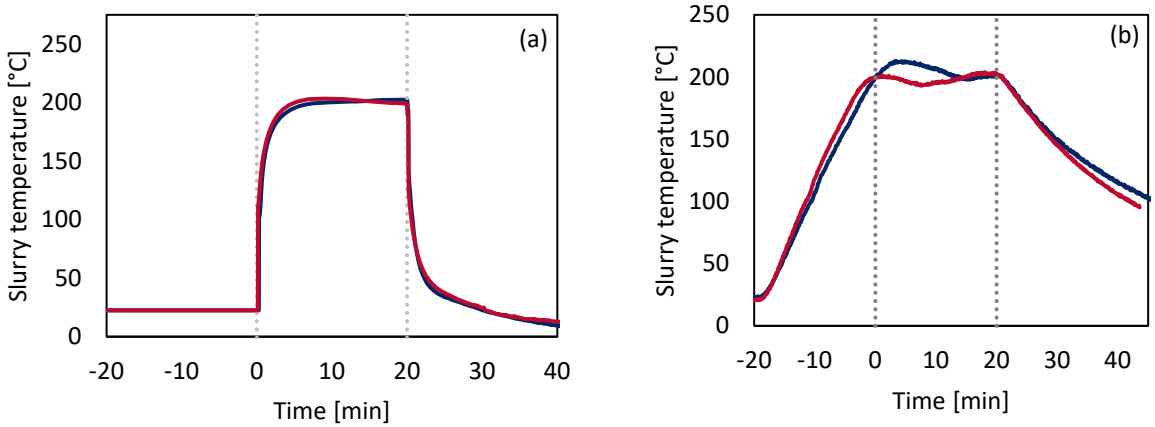

Figure 7. Temperature profiles for slurry (25 g of lignin in 250 mL of n-butanol) vs time for a 20-minute nominal reaction time test show more repeatable thermal profiles for the (a) SBA than for the (b) ICBA.

3.2 Yields of process-solubilized lignin for the ICBA and SBA reactors

Figure 8 plots yields of process-solubilized lignin and THF-insoluble solids versus nominal reaction time for the ICBA and SBA reactors. The control represents yield of process-solubilized lignin from mixture of 10 g lignin in 100 mL of butanol held at room temperature for 30 minutes. Notably, at room temperature, approximately 22% of the lignin was solubilized after 30 minutes with no THF-insoluble solids produced. Heating the mixture of solvent and lignin to 200°C even for zero minutes of reaction time increased the yield of process-solubilized lignin to 45 wt% and 49 wt% for the SBA and ICBA, respectively. The slightly higher yield in the ICBA reflects its longer thermal dwell time, but also it resulted in production of 10 wt% of undesirable THF-insoluble solids compared to none for the SBA.

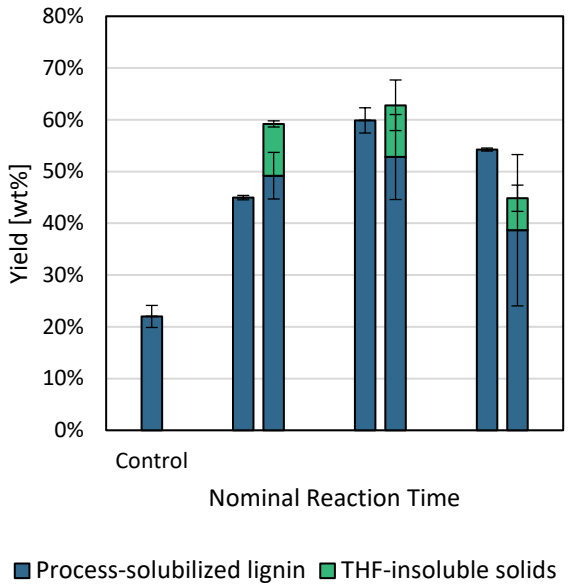

Figure 8. The yield of process-solubilized lignin and THF-insoluble solids changes with differing nominal reaction times for SBA but not with the ICBA. Each trial was performed in duplicate and the error bars represent standard deviation.

For both reactors, the maximum yield of process-solubilized lignin occurs after ten minutes of nominal reaction time, reaching 60 wt% and 53 wt% for the SBA and ICBA,

respectively. Similar to the results at zero minutes of nominal reaction time, the ICBA generates 10 wt% of THF-insoluble solids while none is formed in the SBA reactor. Clearly, the THF-insoluble solids arise from the long thermal dwell times at temperatures less than the set point temperature.

Data from the SBA suggest that experiments with the ICBA greatly underestimated the time required to solubilize lignin when reported as nominal reaction time. The SBA trials also had relatively less uncertainty for the yields of repeated trials than for the ICBA trials. Therefore, SBA trials demonstrated better repeatability than ICBA trials, possibly the result of the superior temperature stability achieved with the SBA.

GC-MS/FID analysis detected no phenolic monomers in process-solubilized lignin, overheads, or THF-soluble solids from either the SBA or ICBA. This result suggests that the solubilized lignin did not decompose into monomers during these SL experiments. To investigate this area further, GPC analysis was performed on the solubilized products from the SBA and ICBA.

3.3 Testing for depolymerization of lignin in the SBA reactor

Using GPC, Figure 9a compares the molecular weight (MW) distributions of the process-solubilized lignin and THF-soluble solids from a 20-minute SBA trial. As previously stated in the methodology section, solids not dissolved in butanol during SL trials that readily dissolved in THF were termed “THF-soluble solids.” Attempting to dissolve these solids in THF served two purposes. It discriminates between what can dissolve in THF (raw lignin and lignin fragments) and what cannot (char-like solid). This idea is further described in the section *Conversion in the ICBA*. Furthermore, GPC requires dissolution in a liquid mobile phase, such as THF. The process-solubilized lignin contained more low MW species than the THF-soluble solids. It

appears that n-butanol was able to dissolve lower MW lignin fractions, which solubilized more effectively as temperature increased from 25°C to 200°C, while larger fractions were insoluble in butanol. It was noted that the chromatograms from process-solubilized lignin and THF-soluble solids, if combined, would resemble the chromatogram of the raw lignin before processing. To observe this phenomenon more clearly, the process-solubilized lignin and THF-soluble solids from each experiment were combined in the same ratios as their yields (this blended sample was referred to as "yield-weighted blend") and analyzed via GPC. The resulting chromatogram of the yield-weighted blend was compared to that obtained from raw lignin feedstock before processing. As shown in Figure 9b, MW distribution for the raw lignin and yield-weighted blend match almost perfectly, indicating that the raw lignin was fractionated without significant depolymerization. (Note that while the heights of the chromatograms differ, only changes in distribution should be compared for GPC.)

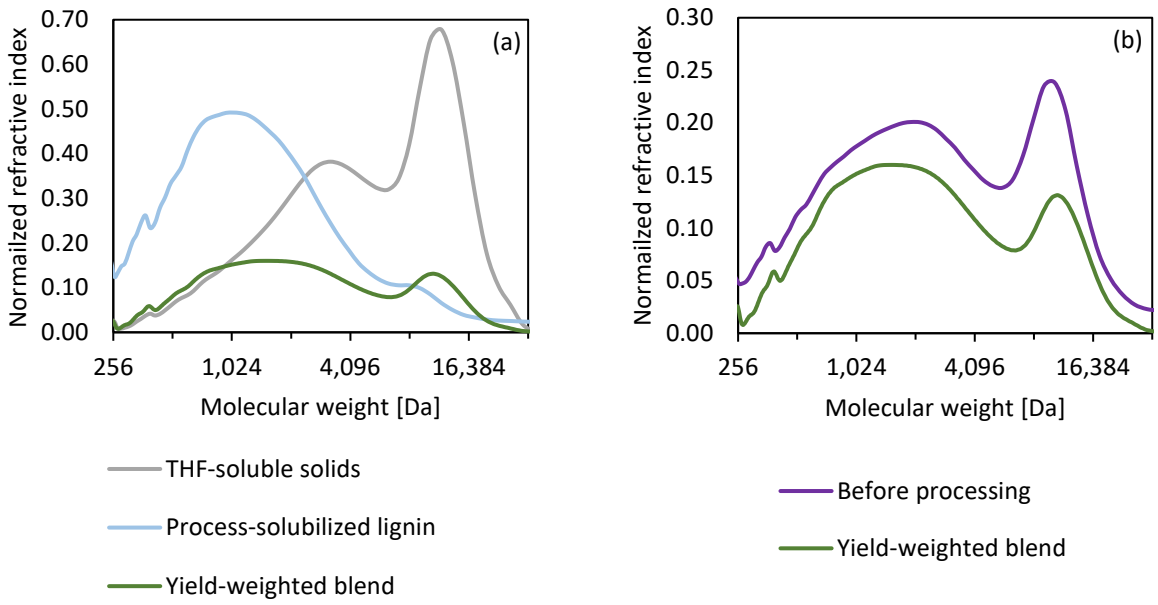

Figure 9. GPC chromatograms of (a) the THF-soluble solids and process-solubilized lignin from a 20-minute SBA trial. (b) GPC chromatograms of a yield-weighted blending of THF-soluble solids and process-solubilized lignin compared to feedstock lignin before processing.

As shown in Table 1, the average MW of the THF-soluble solids (i.e. what butanol did not dissolve) from the control test is higher than the average MW of the raw lignin, demonstrating solubilization during the control trial at room temperature. The THF-soluble solids from the SBA reactor show higher molecular weights than the THF-soluble solids from the control trial or from the raw lignin. It does not appear that repolymerization is responsible for this shift; rather, it reflects fractionation by removal of smaller polymers from the THF-soluble solids sample, which raises the average MW. For the process-solubilized lignin, the average MW does not change substantially between the trials (Table 1), but solubilization improves with increasing reaction time, as illustrated by Figure 8. In other words, the MW distribution of the process-solubilized lignin does not change but the amount of solubilized lignin polymer does.

Table 1. The number (M_n) and weight (M_w) average molecular weights of the THF-soluble solids and process-solubilized lignin differ from the raw lignin, but those of the yield-weighted blends show little difference. Uncertainty expressed as standard error.

		M_n [Da]	M_w [Da]	Dispersity
	Lignin	1291 ± 13	3831 ± 54	2.97 ± 0.05
THF-soluble solids	**Control**	1944 ± 113	5204 ± 200	2.68 ± 0.06
	0 min	2647 ± 97	6767 ± 440	2.56 ± 0.09
	10 min	2261 ± 309	5754 ± 213	2.58 ± 0.26
	20 min	2209 ± 18	5792 ± 233	2.63 ± 0.11
Process-solubilized lignin	**Control**	654 ± 15	1274 ± 91	1.95 ± 0.1
	0 min	692 ± 4	1161 ± 42	1.68 ± 0.06
	10 min	750 ± 46	1374 ± 197	1.83 ± 0.15
	20 min	765 ± 11	1384 ± 80	1.81 ± 0.08
Yield-weighted blends	**Control**	1402 ± 131	4304 ± 152	3.13 ± 0.18
	0 min	1097 ± 7	3728 ± 37	3.4 ± 0.05
	10 min	1021 ± 9	3057 ± 111	2.99 ± 0.08
	20 min	1065 ± 18	3228 ± 58	3.03 ± 0.01

The polymers in the process-solubilized lignin had significantly lower average molecular weights than the THF-soluble solids. This change also manifested itself in polymer dispersity.

Defined by the quotient of the weight average molecular weight (M_w) over the number average molecular weight (M_n), the dispersity represents the heterogeneity of polymer size. The process-solubilized lignin samples had lower dispersity than the THF-soluble solids or the raw lignin, demonstrating that SL dissolves a narrow range of molecular weights (MW). However, when combining the process-solubilized lignin and THF-soluble solids proportionate to their relative yields to obtain the yield-weighted blends, dispersity is not statistically different than for the raw lignin, as assessed by the Student's t-test. Thus, there exists no significant change in distribution between the polymer lengths of the raw lignin and the lignin that underwent SL. The process-solubilized lignin and THF-soluble solids from ICBA experiments were also combined in the same ratios as their yields; comparison of the chromatograms from these combined samples showed no significant change MW distribution from the raw lignin (see Electronic Supplemental Information section 3). Unlike the SBA, the ICBA trials produced a solid that was insoluble in THF and thus could not be analyzed via GPC. This issue prompted analysis of functional groups of the THF-insoluble solids versus the raw lignin.

3.4 Conversion in the ICBA

The SBA achieved superior yields of process-solubilized lignin compared to the ICBA; equally important was the absence of undesirable THF-insoluble solids in SBA products. The solubilized products from the SBA have similar MW distribution as that of the raw lignin, suggesting that solubilization in the SBA hardly modifies the chemical structure of lignin. In contrast, the ICBA converted part of the lignin into a black, char-like solids that adhered to the impeller and thermowell. This hard residue had to be scraped and broken to collect it (see Electronic Supplemental Information section 4). THF did not dissolve this char-like solid, which

was designated THF-insoluble solids. In contrast, the solids recovered from the SBA were friable and soluble in THF.

As evident in Figure 10, solids from the SBA and THF-insoluble solids from the ICBA are visually distinct: Solids from processing lignin in the SBA (Figure 10b) closely resembled solids from raw lignin (Figure 10a). Both were completely soluble in THF. THF-insoluble solids from processing lignin in the ICBA more closely resembled char (Figure 10c).

Figure 10. Solid product from solvent liquefaction of lignin are markedly different for the two reactor systems; (a) Raw lignin after ball milling; (b) solid product from the SBA after 0 minutes of nominal reaction time resembles original lignin; (c) THF-insoluble solids from ICBA reactor after 0 minutes of nominal reaction time resembles char.

FTIR analysis revealed differences in functional groups in the SL products. Figure 11a shows that the spectra of feedstock lignin and THF-soluble solids from the SBA reactor both have broad O-H group stretching at 3400 cm^{-1}, sharp C-H stretching at 2900 cm^{-1}, and aromatic skeletal vibrations at 1600 – 800 cm^{-1} [28–30]. Each product displayed the same or increased O-H group stretching, sharper C-H stretching, and equivalent aromatic vibrations compared to the raw lignin.

FTIR spectra of the THF-insoluble solids from ICBA trials are compared to the feedstock lignin in Figure 11b. Unlike THF-soluble solids, the THF-insoluble solids show decreased O-H group stretching, C-H band stretching, and aromatic skeletal vibrations. The reduction in O-H stretching is strong evidence of dehydration reactions occurring during the ICBA trials to produce THF-insoluble, char-like solid.

The formation of THF-insoluble solids indicates that additional deconstruction reactions occurred during the prolonged thermal dwell time experienced by reactants as they are heated and the products as they are cooled in the ICBA. The THF-insoluble solids are unlikely to be formed by repolymerization because GPC analyses showed no evidence of repolymerization and GC-MS/FID detected no monomers. The likely mechanism is dehydration of lignin to char-like solid at temperatures below the set point temperature where solubilization is promoted [29,31].

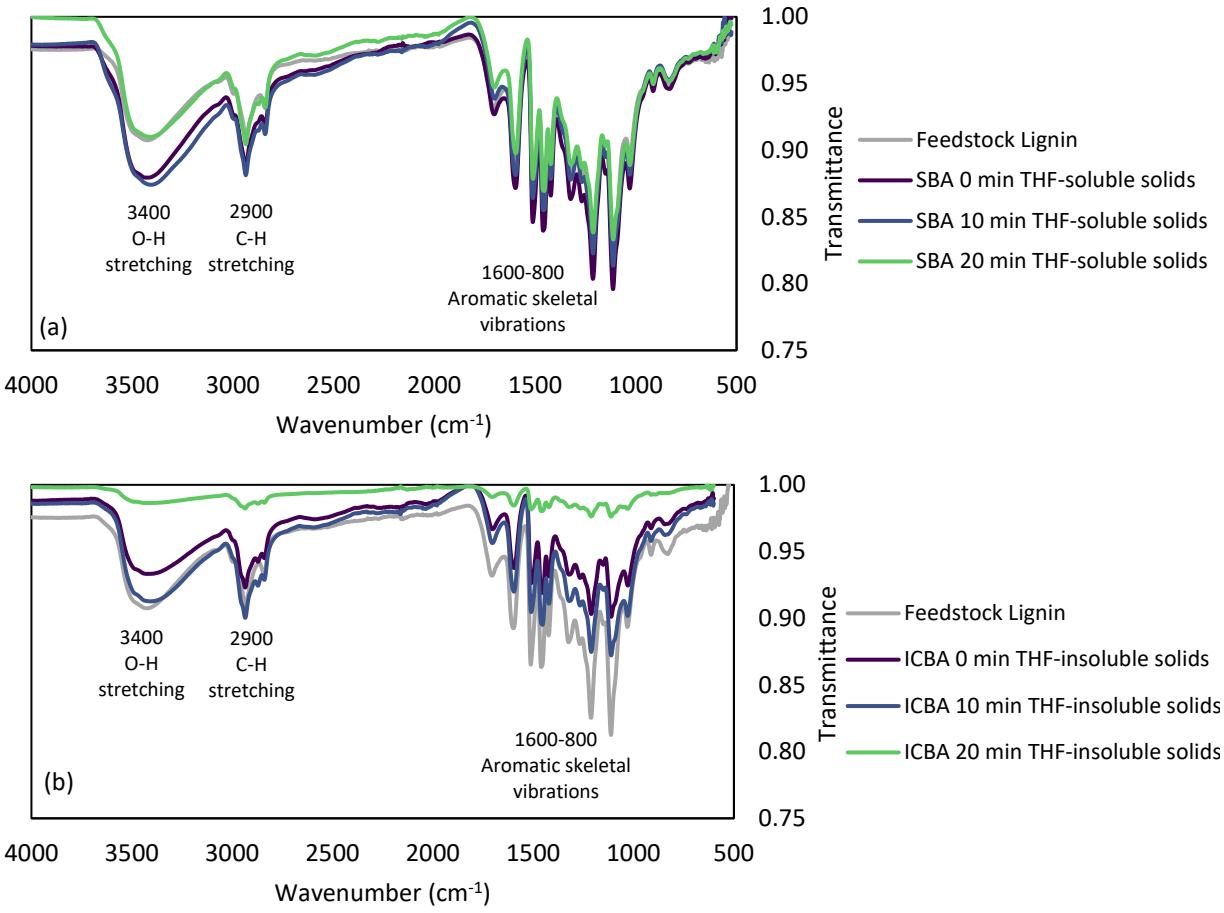

Figure 11. The FTIR spectra of feedstock lignin and the THF-soluble solids from 0-, 10-, and 20-minute SBA trials have similar O-H stretching, C-H stretching, and aromatic skeletal vibrations. (b) The FTIR spectra demonstrates the increased transmittance (reduced absorbance) of char-like solid compared to lignin from the 0-, 10-, and 20-minute ICBA trials.

3.5 Implications for the design of a continuous solvent liquefaction process

The SBA, by closely approximating the temperature profile of a continuous reactor, reduces uncertainty in modeling or designing an industrial process from laboratory data. In contrast, data from the ICBA data underestimates reaction times for an isothermal solvent liquefaction process and thus would result in an undersized industrial-scale continuous reactor.

When designing a continuous plug flow reactor, reactor volume scales linearly with the desired reaction time, biomass throughput, and solvent-to-biomass ratio (Figure 12a). Unlike reactor volume which scales linearly with biomass throughput, costs for unit operations—including reactors—scale logarithmically due to economies of scale (Figure 12b) [32,33].

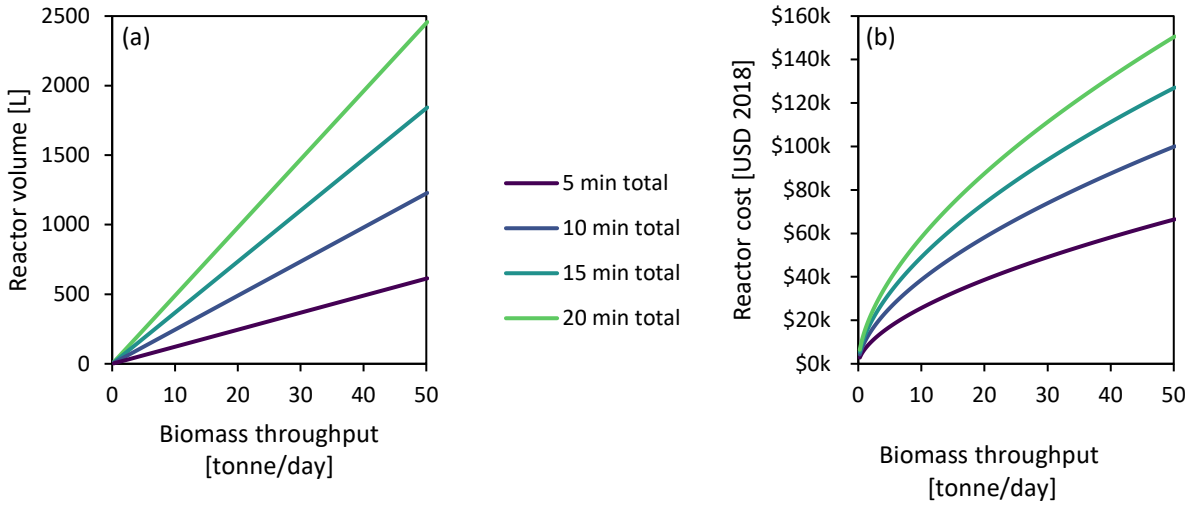

Figure 12. Scaling and economics of solvent liquefaction reactor. (a) Plug flow reactor volume increases linearly with reaction time and biomass throughput for a given solvent-to-biomass ratio. (b) Costs increase logarithmically with reactor throughput according to economies of scales. Note: Cost estimates performed using data and scaling factors from Tables 11-12 and 9-50 from references [32] and [33], respectively.

However, if the biorefinery was designed using skewed small-scale data, the reactor would be undersized. As a result, the biorefinery would need to be operated below its rated capacity to provide sufficient reaction time. Utilizing a reactor below its design capacity introduces a substantial process bottleneck that cascades to both upstream and downstream

equipment, such as pumps and distillation columns, resulting in unused capacity in the other unit operations (Figure 13a). Thus, smaller, less expensive equipment could have been purchased.

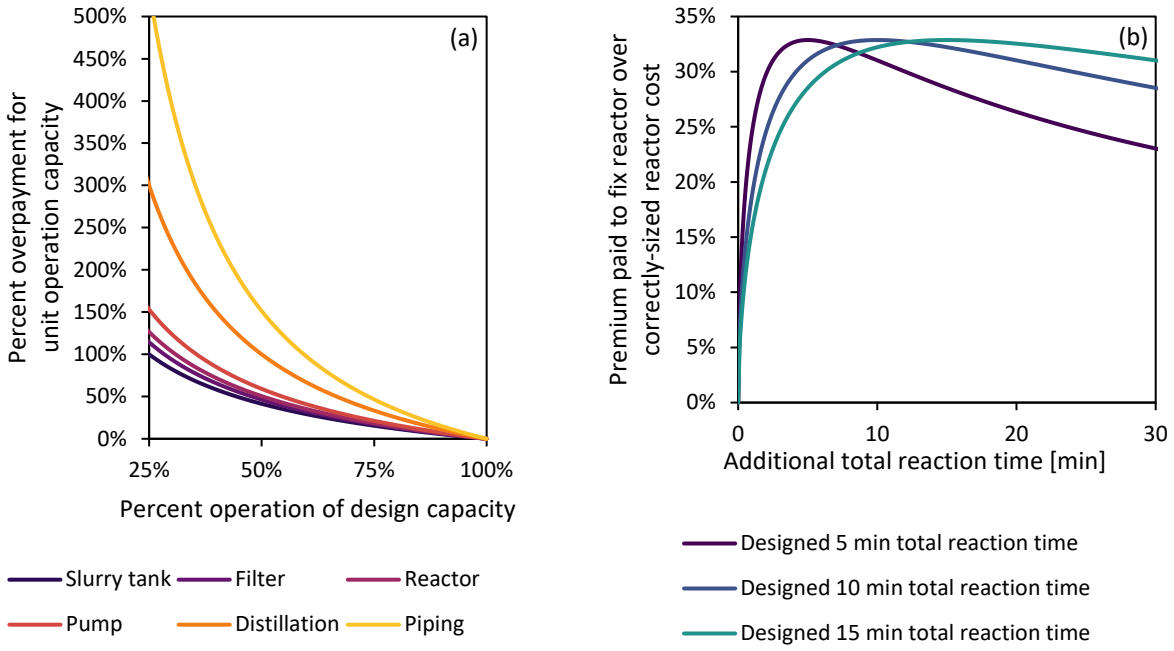

Figure 13. Cost penalties in scaling continuous solvent liquefaction reactors from batch reactor data. (a) Reducing slurry flowrate to increase reaction time uses all unit operations below their design capacity, which is effectively overpaying for each component per unit of capacity. (b) Fixing the reactor by purchasing extra volume supplements reaction time but does not fully capture economies of scale. Note: Scaling factors from Perry and Green [33].

To debottleneck the plant, supplemental reactor volume would be required to reach the desired biomass throughput; however, economies of scale are not fully captured. Purchasing two reactors that combine to provide the desired reaction time is more expensive than purchasing one correctly sized reactor (Figure 13b). (Additional material on purchasing more reactor volume is found in Electronic Supplemental Information section 5.) This additional capital expenditure does not include the likely substantial engineering and retrofitting costs. Simply put, purchasing additional reactor volume to make up for lost capacity is more expensive than buying a correctly designed reactor from the start. Therefore, small-scale data veracity is of paramount importance for the future prospects of industrial solvent liquefaction systems.

4. Conclusions

This study demonstrates the dramatic influence of heating rate on SL of lignin. By isolating this variable, its effects are clear: slow heat transfer can alter product distributions and yields, and apparent reaction rates. Slow heat transfer rates and experimental results cannot be decoupled. Rapid heat transfer, expected in continuous systems, is therefore essential for small-scale experiments. The novel SBA system overcomes the limitations of slow heat transfer rates and therefore better approximates the thermal profile of a continuous system. Results from the ICBA substantially underestimated the volume needed for a continuous reactor. This error would negatively impact the economic efficiency of each biorefinery unit operation unless corrected.

Acknowledgements

The authors appreciate the work of Andrew Friend, Martin Haverly, Zachary Paskach, and Lysle Whitmer for constructing a previous iteration of the SBA and assisting with subsequent upgrades for these experiments.

Author contributions

J.K.L., A.G., P.G., R.G.S., and R.C.B. conceptualized the SBA. P.G. primarily designed the system. J.K.L. and P.G. performed SBA shakedown and preliminary testing. J.K.L. and J.L.B. completed the SBA and ICBA experiments. J.K.L., J.L.B., C.A.P., A.G., and S.A.R. analyzed the products. J.K.L., J.L.B., and S.A.R. performed process calculations. P.D.K., M.D.B., E.J.M.H., P.G., and R.G.S. determined initial experimental parameters. J.K.L. and J.L.B. wrote the article with input from all authors.

Funding sources

This work was funded by Vertoro B.V., Gary and Donna Hoover Endowment at Iowa State University, and RAPID Institute, which is sponsored by the United States Department of Energy and administrated by the American Institute of Chemical Engineers (AIChE).

Conflict of Interest

P.D.K. and M.D.B. work at and founded Vertoro B.V., which primarily funded this work. E.J.M.H acts as scientific advisor to Vertoro B.V.

References

[1] A. Ghosh, M.R. Haverly, Solvent Liquefaction, in: R.C. Brown (Ed.), Thermochem. Process. Biomass Convers. into Fuels, Chem. Power, 2nd ed., John Wiley and Sons, 2019: pp. 257–306.

[2] J.K. Lindstrom, A. Shaw, X. Zhang, R.C. Brown, Condensed phase reactions during thermal deconstruction, in: R.C. Brown (Ed.), Thermochem. Process. Biomass Convers. into Fuels, Chem. Power, 2nd ed., John Wiley and Sons, 2019: pp. 17–48.

[3] M.R. Haverly, K. V. Okoren, R.C. Brown, Optimization of Phenolic Monomer Production from Solvent Liquefaction of Lignin, ACS Sustain. Chem. Eng. 6 (2018) 12675–12683. doi:10.1021/acssuschemeng.8b01629.

[4] J.K. Lindstrom, A. Ghosh, S. Rollag, R.C. Brown, Production of sugars from lignocellulosic biomass: a critical review of biological and thermochemical routes, Submitted. Submitted (2020).

[5] K.H. Kim, R.C. Brown, M. Kieffer, X. Bai, Hydrogen-donor-assisted solvent liquefaction of lignin to short-chain alkylphenols using a micro reactor/gas chromatography system, Energy and Fuels. 28 (2014) 6429–6437. doi:10.1021/ef501678w.

[6] M.R. Haverly, A. Ghosh, R.C. Brown, The effect of moisture on hydrocarbon-based solvent liquefaction of pine, cellulose and lignin, J. Anal. Appl. Pyrolysis. 146 (2020). doi:10.1016/j.jaap.2019.104758.

[7] M.R. Haverly, T.C. Schulz, L.E. Whitmer, A.J. Friend, J.M. Funkhouser, R.G. Smith, M.K. Young, R.C. Brown, Continuous solvent liquefaction of biomass in a hydrocarbon solvent, Fuel. 211 (2018) 291–300. doi:10.1016/j.fuel.2017.09.072.

[8] J.G. Costandy, T.F. Edgar, M. Baldea, Switching from Batch to Continuous Reactors Is a Trajectory Optimization Problem, Ind. Eng. Chem. Res. 58 (2019) 13718–13736. doi:10.1021/acs.iecr.9b01126.

[9] D.C. Elliott, P. Biller, A.B. Ross, A.J. Schmidt, S.B. Jones, Hydrothermal liquefaction of biomass: Developments from batch to continuous process, Bioresour. Technol. 178 (2015) 147–156. doi:10.1016/j.biortech.2014.09.132.

[10] L. Qian, S. Wang, P.E. Savage, Hydrothermal liquefaction of sewage sludge under isothermal and fast conditions, Bioresour. Technol. 232 (2017) 27–34. doi:10.1016/j.biortech.2017.02.017.

[11] A. Ghosh, R.C. Brown, Factors Influencing Cellulosic Sugar Production during Acid-Catalyzed Solvent Liquefaction in 1,4-Dioxane, ACS Sustain. Chem. Eng. (2019). doi:10.1021/acssuschemeng.9b05108.

[12] A. Ghosh, R.C. Brown, X. Bai, Production of solubilized carbohydrate from cellulose using non-catalytic, supercritical depolymerization in polar aprotic solvents, Green Chem. 18 (2016) 1023–1031. doi:10.1039/c5gc02071a.

[13] W.J. Connors, L.N. Johanson, K. V. Sarkanen, P. Winslow, Thermal degradation of kraft lignin in tetralin, Holzforschung. 34 (1980) 29–37. doi:10.1515/hfsg.1980.34.1.29.

[14] S. Kumar, J.P. Lange, G. Van Rossum, S.R.A. Kersten, Liquefaction of lignocellulose: Process parameter study to minimize heavy ends, Ind. Eng. Chem. Res. 53 (2014) 11668–11676. doi:10.1021/ie501579v.

[15] F. De Miguel Mercader, M.J. Groeneveld, S.R.A. Kersten, C. Geantet, G. Toussaint, N.W.J. Way, C.J. Schaverien, K.J.A. Hogendoorn, Hydrodeoxygenation of pyrolysis oil fractions: Process understanding and quality assessment through co-processing in refinery units, Energy Environ. Sci. 4 (2011) 985–997. doi:10.1039/c0ee00523a.

[16] J.B. Nielsen, A. Jensen, L.R. Madsen, F.H. Larsen, C. Felby, A.D. Jensen, Noncatalytic Direct Liquefaction of Biorefinery Lignin by Ethanol, Energy and Fuels. 31 (2017) 7223–7233. doi:10.1021/acs.energyfuels.7b00968.

[17] Z. Liu, F.-S. Zhang, Effects of various solvents on the liquefaction of biomass to produce fuels and chemical feedstocks, Energy Convers. Manag. 49 (2008) 3498–3504. doi:10.1016/j.enconman.2008.08.009.

[18] S. Kumar, A. Segins, J.P. Lange, G. Van Rossum, S.R.A. Kersten, Liquefaction of Lignocellulose in Light Cycle Oil: A Process Concept Study, ACS Sustain. Chem. Eng. 4 (2016) 3087–3094. doi:10.1021/acssuschemeng.6b00055.

[19] B. Zhang, M. Von Keitz, K. Valentas, Thermal effects on hydrothermal biomass liquefaction, Appl. Biochem. Biotechnol. 147 (2008) 143–150. doi:10.1007/s12010-008-8131-5.

[20] D.R. Vardon, B.K. Sharma, G. V. Blazina, K. Rajagopalan, T.J. Strathmann, Thermochemical conversion of raw and defatted algal biomass via hydrothermal liquefaction and slow pyrolysis, Bioresour. Technol. 109 (2012) 178–187. doi:10.1016/j.biortech.2012.01.008.

[21] D. Brodzki, A. Abou-Akar, G. Djèga-Mariadassou, C.Z. Li, B. Xu, R. Kandiyoti, Liquefaction of coal and maceral concentrates in a stirred micro-autoclave and a flowing-solvent reactor, Fuel. 73 (1994) 1331–1337. doi:10.1016/0016-2361(94)90309-3.

[22] F. Behrendt, Y. Neubauer, M. Oevermann, B. Wilmes, N. Zobel, Direct Liquefaction of Biomass, Chem. Eng. Technol. 31 (2008) 667–677. doi:10.1002/ceat.200800077.

[23] Renmatix, Omno Polymers, (2020) 2020.

[24] I.H. Bell, J. Wronski, S. Quoilin, V. Lemort, Pure and Pseudo-pure Fluid Thermophysical Property Evaluation and the Open-Source Thermophysical Property Library CoolProp, Ind. Eng. Chem. Res. 53 (2014) 2498–2508. doi:10.1021/ie4033999.

[25] Y.S. Choi, P.A. Johnston, R.C. Brown, B.H. Shanks, K.H. Lee, Detailed characterization of red oak-derived pyrolysis oil: Integrated use of GC, HPLC, IC, GPC and Karl-Fischer, J. Anal. Appl. Pyrolysis. 110 (2014) 147–154. doi:10.1029/EO068i018p00498.

[26] P. Kouris, E. Hensen, M. Boot, H. Oevering, (Patent No. WO2019053287), A method for obtaining a stable lignin : polar organic solvent composition via mild solvolytic

modifications, (2019).

[27] P.D. Kouris, D.J.G.P. van Osch, G.J.W. Cremers, M.D. Boot, E.J.M. Hensen, Mild thermolytic solvolysis of technical lignins in polar organic solvents to a crude lignin oil, Sustain. Energy Fuels. (2020) 6212–6226. doi:10.1039/d0se01016b.

[28] R. Briones, L. Serrano, R. Llano-Ponte, J. Labidi, Polyols obtained from solvolysis liquefaction of biodiesel production solid residues, Chem. Eng. J. 175 (2011) 169–175. doi:10.1016/j.cej.2011.09.090.

[29] R.K. Sharma, J.B. Wooten, V.L. Baliga, X. Lin, W.G. Chan, M.R. Hajaligol, Characterization of chars from pyrolysis of lignin, Fuel. 83 (2004) 1469–1482. doi:10.1016/j.fuel.2003.11.015.

[30] M.R. Haverly, K. V. Okoren, R.C. Brown, Thermal Stability of Fractionated Bio-Oil from Fast Pyrolysis, Energy and Fuels. 30 (2016) 9419–9426. doi:10.1021/acs.energyfuels.6b01606.

[31] D. Chen, A. Gao, K. Cen, J. Zhang, X. Cao, Z. Ma, Investigation of biomass torrefaction based on three major components : Hemicellulose , cellulose , and lignin, Energy Convers. Manag. 169 (2018) 228–237. doi:10.1016/j.enconman.2018.05.063.

[32] D.W. Green, R.H. Perry, eds., Perry's Chemical Engineering Handbook, 8th ed., McGraw-Hill Companies, Inc., 2008.

[33] R.H. Perry, D.W. Green, Perry's Chemical Engineering Handbook, 7th ed., McGraw-Hill Professional, 1997.